Article:
Matam, S.K., Boudjema, L., Quesne, M.G. et al. (2025) A complementary experimental and computational study on methanol adsorption isotherms of H-ZSM-5. Physical Chemistry Chemical Physics, 27 (5). pp. 2601-2614. ISSN: 1463-9076

https://doi.org/10.1039/d4cp03761h

A complementary experimental and computational study on methanol adsorption isotherms of H-ZSM-5

Santhosh K. Matam[1,2,*], Lotfi Boudjema[1,3,4], Matthew Quesne[1,2,5],

James Taylor[6], C. Richard A. Catlow[1,2,3]

[1]UK Catalysis Hub, Research Complex at Harwell, Science and Technology Facilities Council, Rutherford Appleton Laboratory, OX11 0FA, UK

[2]Cardiff Catalysis Institute, School of Chemistry, Cardiff University, Cardiff, CF10 3AT, UK

[3]Department of Chemistry, University College London, 20 Gordon St., London WC1E 6BT, UK

[4]ICGM, Univ. Montpellier, CNRS, ENSCM, Montpellier, France

[5]School of Chemistry, University of Leeds, Leeds LS2 9JT, UK

[6]ISIS Pulsed Neutron and Muon Facility, Science and Technology Facilities Council, Rutherford Appleton Laboratory, OX11 0QX, UK

*Corresponding author: santhosh.matam@rc-harwell.ac.uk;

Website: www.ukcatalysishub.co.uk

Abstract

Methanol adsorption isotherms of fresh f-ZSM-5 and steamed s-ZSM-5 (Si/Al ≈ 40) are investigated experimentally at room temperature under equilibrium and by Grand Canonical Monte Carlo (GCMC) simulations with the aim of understanding the adsorption capacity, geometry and sites as a function of steam treatment (at 573 K for 24h). Methanol adsorption energies calculated by GCMC are complemented by density functional theory (DFT) employing both periodic and quantum mechanics/molecular mechanics (QM/MM) techniques. Physical and textural properties of f-ZSM-5 and s-ZSM-5 are characterised by diffuse reflectance infrared Fourier transformed spectroscopy (DRIFTS) and N_2-physisorption, which form a basis to construct models for f-ZSM-5 and s-ZSM-5 to simulate methanol adsorption isotherms by GCMC. Both Brønsted and silanol hydroxyls are observed in f-ZSM-5 and s-ZSM-5 by DRIFTS; however, these species, especially Brønsted species, decreased considerably upon steam treatment in s-ZSM-5 due to dealumination. Although the total pore volume and mesoporosity increased in s-ZSM-5 as compared in f-ZSM-5, the total surface area (375 m^2/g) of the steamed zeolite is lower than the fresh zeolite (416 m^2/g) due to pore plugging caused by partial dislodgement of framework Al on steam treatment. Implications of the steam treatment on the methanol adsorption capacity of the zeolites are reflected in the experimental methanol adsorption isotherms, collected (in the pressure range between 0 and 12 kPa) at room temperature under equilibrium, which find that the overall methanol uptake is lower for s-ZSM-5 than for f-ZSM-5. The GCMC simulations show that the nature, location and distribution of acidic hydroxyls determine the methanol adsorption capacity, geometry and hence the isotherm profiles of f-ZSM-5 and s-ZSM-5. The GCMC simulations provide insight on the different adsorption sites and their reactivity towards methanol which paves the way not only to describe the isotherms of f-ZSM-5 and s-ZSM-5 but also offers a means to understand better the deactivation of ZSM-5 by steam (leading to dealumination) and subtle differences in surface adsorbed species on ZSM-5 procured from different sources.

Key words: H-ZSM-5; hydroxyls; methanol; adsorption; isotherms; GCMC; DFT; QM/MM

1. Introduction

ZSM-5 is crucial in many chemical and environmental technologies owing to its unique porous architecture with Brønsted acid sites which catalyse various key reactions, including the widely investigated methanol to hydrocarbon process [1-4]. The reactivity of methanol in H-ZSM-5 pores is especially intriguing, particularly under ambient conditions [5-17]. Several studies by infrared, NMR and simulations indicate different species and processes, including methanol hydrogen bonded with Brønsted hydroxyls [6] and methoxylated framework oxygen at the Brønsted site [5,11]; and indeed our recent studies demonstrate the occurrence of both hydrogen bonded methanol and methoxylation [12,13]. The extent of methoxylation and the geometry of hydrogen bonded methanol, which can be either neutral or protonated, are dependent on the methanol loading per Brønsted site [6,10,13]. Computational studies confirm the occurrence of hydrogen bonded methanol with the two geometries depending on the methanol loading and consistently indicate that methanol loading ≥ 2 per Brønsted sites decreases the energy barrier for the methoxylation step but they have not, as yet, found a complete removal of the barrier [7,8,14-17]. Moreover, the majority of studies on diffusion of methanol in ZSM-5 pores by Quasi Elastic neutron Scattering (QENS) conducted under equilibrium conditions conclude that the adsorbed methanol is immobile under ambient conditions [18-21], although one study reports a very slow methanol diffusion with a self-diffusion co-efficient of 10^{-11} m^2/s [22]. Although the discrepancies between the QENS studies can be explained to some extent by the instrumental resolution, the fundamental physical and chemical aspects of methanol adsorption and diffusion still have many uncertainties.

Adsorption isotherms which are sensitive to adsorption sites and the type of adsorption, (physisorption or chemisorption [23]) and the adsorption geometry of the probe molecule, can shed light on the physical and chemical aspects of methanol structure and dynamics in H-ZSM-5 pores under ambient conditions. To this end, we have combined experiment and molecular simulations to probe the adsorption of methanol in H-ZSM-5 pores. No such a detailed study has been reported previously, and our work will, moreover, complement previous studies of the effect of the alkali cation in ZSM-5 on the interaction with methanol [24,25], where the methanol desorption energies derived by temperature programmed desorption (TPD) and the desorption energy heterogeneity of H-ZSM-5 and Na-ZSM-5 correlated with methanol adsorption isotherms obtained by gravimetric method [24].

Grand Canonical Monte Carlo (GCMC) simulations are effective for describing and predicting the adsorption isotherms and thermodynamics of molecules in porous zeolites [26-28] such as

methanol in ZSM-5. For example, the adsorption thermodynamics of benzene and p-xylene in silicalite are accurately predicted by GCMC simulations [28]. Also, other studies employed GCMC to simulate interactions between different adsorbates and adsorbents such as that of chlorinated hydrocarbons in zeolites [29], benzene and propene in MCM-22 [30], and methanol, toluene, ethylbenzene and styrene in zeolites [31]. These studies demonstrate the importance of GCMC simulations to understand the adsorption of molecules in zeolites [32]. However, no studies to date employed GCMC simulations in combination with experiments to understand the intriguing behaviour of methanol adsorption phenomenon in H-ZSM-5 pores under ambient conditions. In this study further insight is obtained by DFT and quantum mechanics/molecular mechanics (QM/MM) calculations of the structures and energies of adsorbed configurations because GCMC is inadequate to describe charge transfer between the Brønsted acidic site and methanol. Therefore, QM/MM and periodic calculations using Perdew-Burke-Ernzerhof (PBE) are employed to examine single methanol molecule adsorption on an individual active site and multiple methanol molecules adsorption in a unit cell, respectively.

The aim of the present work is therefore to describe the experimental methanol adsorption isotherms of H-ZSM-5 as a function of steam treatment, which is commonly used in preparing ZSM-5 catalysts for some industrial applications [33], and to gain molecular information on the adsorption sites of the zeolite, adsorption geometry of methanol and adsorption energies. The results show that methanol adsorption is sensitive to methanol loading, the adsorption site of ZSM-5 and the adsorption geometry. The results highlight the significant effects of steam de-alumination on the adsorptive properties of the material.

2. Materials and methods

2.1 *Zeolite H-ZSM-5:*

Zeolite NH_4-ZSM-5 with Si/Al of 40 was purchased from Zeolyst International, Inc. The zeolite was calcined in air at 500 °C for 24 h to obtain H-ZSM-5, denoted as fresh H-ZSM-5 (f-ZSM-5). The fresh zeolite was subjected to steaming at 500 °C for 24 h under steam and N_2 flow (100 ml/min). The steamed zeolite is referred to as s-ZSM-5.

2.2 *Diffuse reflectance infrared Fourier transform spectroscopy (DRIFTS):*

Infrared spectra were collected using Bruker Vertex 80 spectrometer equipped with a Harrick Praying Mantis cell connected to a gas feeding system comprising mass flow controllers. The zeolites were dehydrated at 500 °C for 2 h by flowing boiled-off N_2 (50 ml/min) and cooled to

200 °C under the same flow and, the spectra were recorded by taking 64 scans with a resolution of 4 cm^{-1} using a liquid nitrogen cooled MCT detector.

2.3 *Nitrogen physisorption:*

Nitrogen adsorption – desorption isotherms were collected at –196 °C on a Quadrasorb EVO instrument (Model QDS-30). Prior to the experiments, the zeolites were outgassed at 300 °C for 15 h. The micro pore volume (V_{micro}) and meso pore surface area (S_{meso}) were determined by the *t*-plot method. The total surface area (S_{total}) of the zeolites was determined by the Brunauer–Emmett–Teller (BET) method [34].

2.4 *Methanol adsorption isotherms:*

Methanol adsorption isotherms were collected at room temperature (20 °C) on an automated Quantachrome Autoadsorb IQ Chemi. The manifold was at 50 °C and the bath temperature was at 20 °C. Prior to each adsorption measurement, the zeolites were outgassed at 300 °C for 12 h to remove any adsorbed moisture and other gaseous molecules.

2.5 *Computational studies:*

2.5.1 Isotherm Modelling

Construction of H-ZSM-5 models

The framework of H-ZSM-5 with Si/Al of 40 was constructed (Fig. S1, Supporting Information (SI)) using the crystallographic data [35]. A single unit cell of the MFI structure contains 96 Si and 192 O atoms with dimensions of 20.35 Å × 20.22 Å × 13.6 Å [12,23]. To obtain the desired Si/Al ratio of H-ZSM-5, Si atoms at different crystallographic T-sites were substituted with Al atoms by applying Lowenstein's rule [36]. Two models were constructed, each for the fresh and steamed ZSM-5 to simulate methanol adsorption isotherms of the zeolites and are discussed in section 3.4. Additionally, two more models with varied acidic hydroxyls at different crystallographic sites were tested to show the effect of nature and location of hydroxyls on the methanol adsorption profiles (Fig. S2). More details of the Al and Brønsted acid site distributions will be given below and provided in SI.

Point charges were assigned to f-ZSM-5 and s-ZSM-5 models to represent the complex electrostatic potential of the zeolite, including multipole interactions. The Density Derived Electrostatic and Chemical (DDEC6) approach was applied to obtain atomic net charges for both f-ZSM-5 and s-ZSM-5 structures [37]. The density functional theory (DFT) calculations were conducted using the Vienna Ab initio Simulation Package (VASP, version 5.4.1) to derive

atomic charges [38]. The automatic mesh generation based on Monkhorst-pack method was used for Brillouin zone sampling and the k-point grid was set to 2×2×2 for structures [39,40]. All calculations were carried out at the Perdew-Burke-Ernzerhof (PBE) generalized gradient approximation (GGA) level with a plane-wave cut-off of 550 eV [39,40]. Structures used for charge analysis were optimized by self-consistent field (SCF) electronic energies with a convergence criterion of 10^{-5} eV [41]. Then, single-point calculations were conducted to generate required AECCAR0, AECCAR2, and CHGCAR files for performing DDEC6 atomic population analysis (Tables S1 and S2).

Force Fields

The intramolecular interactions in the fresh and steamed ZSM-5 structures were described by the forcefield of Schroder et al. [42]. The intermolecular interactions between all the ZSM-5 atoms and oxygen and hydrogen atoms of the methanol molecule were described by the Lennard Jones (LJ) 12-6 potential (Figures S3, S4 and S5 and Tables S1, S2, S3 and S4). The Lennard Jones potential parameters were taken from [43, 44] and are widely employed due to their accurate description of the methanol adsorption in zeolites [45-47]. The charges of methanol were determined by a Mulliken population analysis calculated by *ab initio* DFT approach as reported in Blanco et al. [44] (Table S5). The electrostatic interactions were calculated using Ewald summation and a cut-off distance of 12 Å was employed to evaluate the short-range interactions. The Ewald precision was set at 1.0×10^{-6} kcal mol^{-1}.

Grand Canonical Monte Carlo (GCMC) calculations

GCMC simulations were conducted in a simulation box of 2×2×2 unit cell by Dl-Monte program [48]. The periodic boundary conditions were applied in 3D. A spherical cut-off radius of 12 Å was applied for Lennard Jones interactions [49]. The simulations were conducted with four Monte Carlo moves: (i) molecular displacement, (ii) molecular rotation, (iii) insertion of a molecule with random orientation into a random position in the system and (iv) the deletion of a randomly chosen methanol molecule from the system [50]. The simulations were carried out with 1.0×10^6 Monte Carlo steps for the production and 3×10^6 steps for the equilibration [51]. By employing the GCMC approach, the isosteric heat of adsorption is calculated by the expression, $Q = RT - \left(\frac{\partial \langle v \rangle}{\partial \langle q \rangle}\right)_T$ where $\langle v \rangle$ is the potential average of adsorbed phase and $\langle q \rangle$ is the average uptake at temperature T and R is the gas constant [52,53].

2.5.2 Methanol adsorption energies

To calculate adsorption energies, both periodic and Quantum Mechanical/Molecular Mechanical (QM/MM) methods were used. Periodical DFT calculations were performed on the whole unit cell of both f-ZSM-5 and s-ZSM-5 to access the behaviour of the sample at different methanol loadings with explicit inclusion of all long-range perturbations from multiple silanol and Brønsted acid sites in each model. The QM/MM calculations were used to access better adsorption to specific sites with a higher level of QM-methodology and to rationalises localised active site effects.

Periodical DFT calculations

The DFT calculations using periodic boundary conditions techniques were conducted by following the well established and benchmarked protocols [54]. The binding energies were produced by subtracting the energies of methanol and the bare f-ZSM-5 or s-ZSM-5 zeolite without methanol in the gas phase from the energy of methanol bound systems. For each model a full unit cell containing all modifications to the zeolite lattice was used. The PBE [55] in combination with plane-wave basis set (applied to all valence electrons) was implemented inside the VASP code [56-58]. Core-electrons were simulated via the projected augmented wave method (PAW) [59], whilst the effects of long range non-bonding [56] interactions were included using the Grimme D3 dispersion method [60, 61]. A fine Monkhorst-Pack grid (Kpoint 5x5x5) was utilized for the energetics. An electronic threshold of 10^{-5} eV was set for convergence of the SCF whilst the ionic relaxation convergence was set to 0.01 eV for geometry optimization. No co-ordinates were fixed during the optimization of each intermediate and all energies reported here were derived by a combination of the Blöchl tetrahedron smearing method [62] and a plane-wave cut-off of 520 eV.

Quantum mechanics/molecular mechanics (QM/MM) calculations

QM/MM protocols utilizing the ChemShell code [63,64] as a platform to simulate methanol adsorption in zeolitic aluminosilicates has demonstrated excellent convergence between experimentally derived values and those obtained by the embedded cluster models [65,66]. Therefore, such a scheme was used in this study, whereby, the unit cell of MFI [67] was extended to a sphere of 40 angstroms in radius around the Brønsted acid and silanol hydroxyls of interest. Four QM-regions were considered and are shown in Fig. 1. These models consisted of: (A) f-ZSM-5 with one methanol bound to T7 (silanol), (B) two methanol molecules bound to T8 (Brønsted), (C) s-ZSM-5 one methanol molecule bound to T7 (silanol) and (D) two methanol molecules bond to T10 (Brønsted). The MM-energies were calculated by dl-poly [68]

using the forcefield developed by Hill and Sauer [69] with an electrostatic embedding scheme also being employed to compensate for changes in the QM-region. Orca [70] in combination with the B3LYP functional and the triplet-ζ basis set TZVP was used for the QM-region.

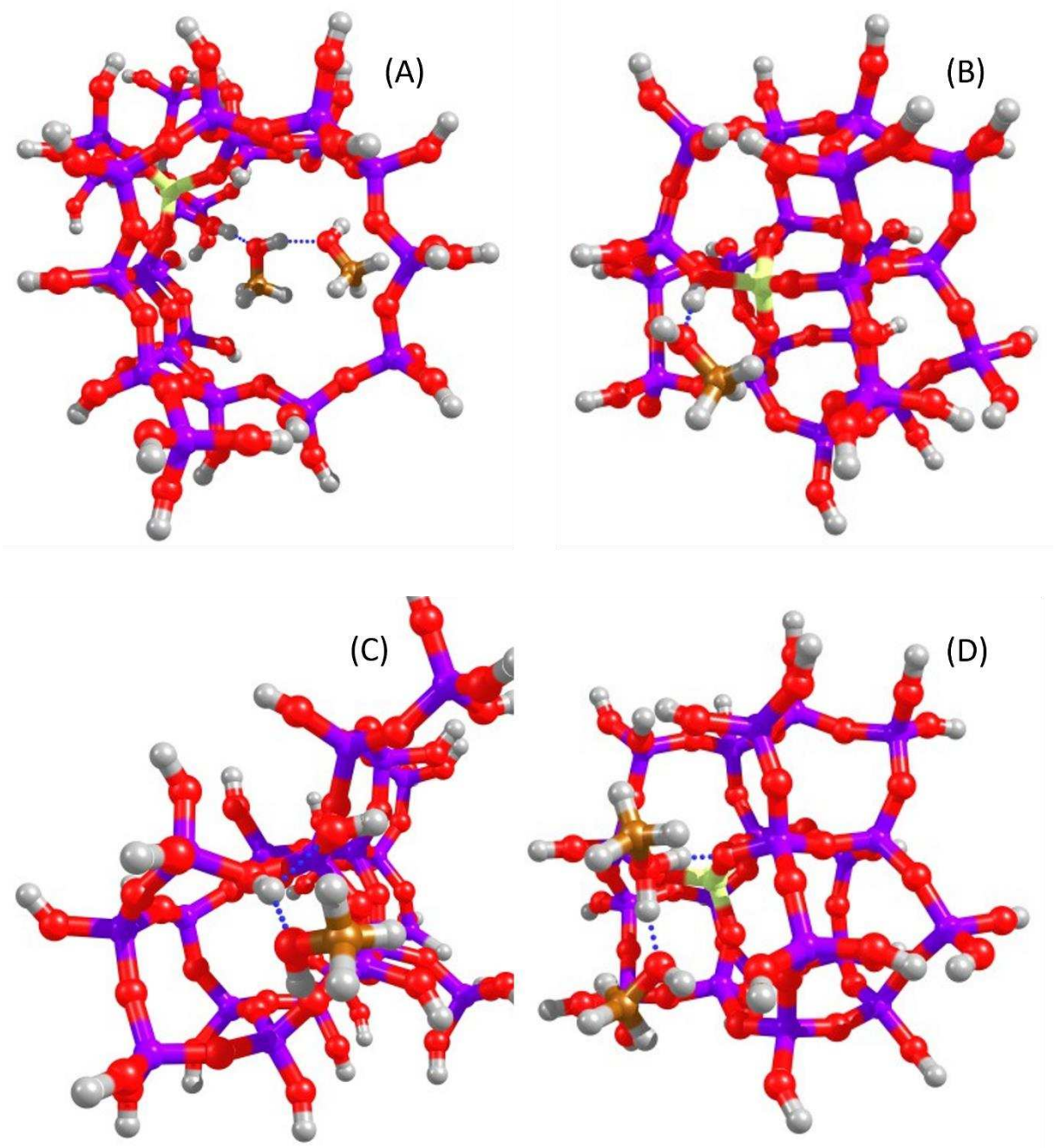

Fig. 1. QM-clusters used in the QM/MM calculations of methanol adsorption in f-ZSM-5 (A and B) and s-ZSM-5 (C and D). Two methanol molecules adsorbed to a combination of T8 Brønsted site and T9 silanol (A), one methanol molecule adsorbed to the T10 Brønsted site (B), one methanol molecule adsorbed to a combination of T7 and T10 silanols (C), two methanol molecules adsorbed to the T10 Brønsted site (D). The blue, yellow, red and gray denote Si, Al, O and H, respectively.

3. Results and discussion

3.1 *Diffuse reflectance infrared Fourier transform spectroscopy (DRIFTS):*

The fresh and steamed zeolites were characterized by DRIFTS to probe the nature of acidic hydroxyls of the zeolites and effect of steam treatment on the nature and distribution of these hydroxyls [6,10,12,13]. The dehydration of the zeolites leads to well resolved bands at 3735 and 3604 cm^{-1} which are characteristic of O – H stretching modes (Fig. 2). The bands at 3735 and 3604 cm^{-1} are attributed to silanol and Brønsted acidic hydroxyls, respectively [6,10,12,13]. In the f-ZSM-5 spectrum, a shoulder to the prominent band at 3604 cm^{-1} appeared at 3500 cm^{-1} and is assigned to the rehydration of a fraction of acidic hydroxyls on cooling after dehydration at 500 °C. In a marked contrast, the shoulder does not appear for the steamed zeolite, indicating that such a rehydration process does not take place in s-ZSM-5 under these experimental conditions [12,13]. It implies that the steam treatment might have dislodged easily accessible Al sites, and hence a loss of a fraction of acidic hydroxyls [20].

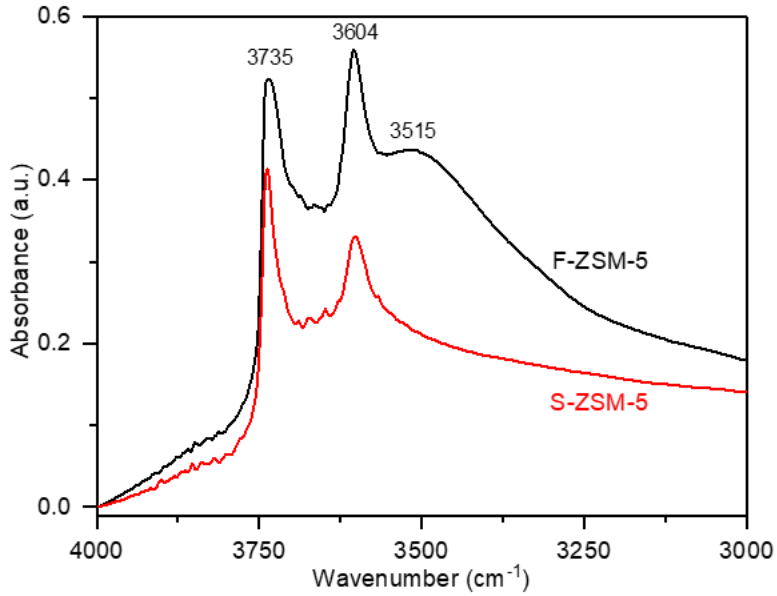

Fig. 2. DRIFTS of fresh and steamed zeolites collected at 200 °C. The spectra are normalised to the framework band at 1880 cm^{-1}.

In line with these observations, the relative intensity of the hydroxyl bands, especially the band at 3604 cm^{-1}, decreases for the steamed as compared to the fresh zeolite. It is well known that either steam treatment or reaction conditions that generate considerable steam (like MTH reaction) promotes hydrolysis of framework Al–O–Si bonds leading to dealumination [20,71,72]. From DRIFTS data it is evident that f-ZSM-5 and s-ZSM-5 contain both Brønsted and silanol hydroxyls, and a significant proportion of the hydroxyls decreases, especially the easily accessible Brønsted acidic hydroxyls, upon steam treatment. The effect of steam

treatment on the physical and textural properties of the zeolites were next studied by N_2 physisorption.

3.2 N_2 physisorption:

The N_2 adsorption and desorption isotherms of fresh and steamed ZSM-5 are shown in Fig. 3. According to the IUPAC classification, the isotherms are assigned to type I [73,74]. It is evident from the f-ZSM-5 isotherm that there is a steep nitrogen uptake at lower, and a gradual nitrogen uptake at higher relative partial pressures, which is typical for microporous materials. In line with this observation, the surface area of f-ZSM-5 is mainly (~84%) due to micropores and a contribution from the mesopores to the total surface area is relatively small (Table 1).

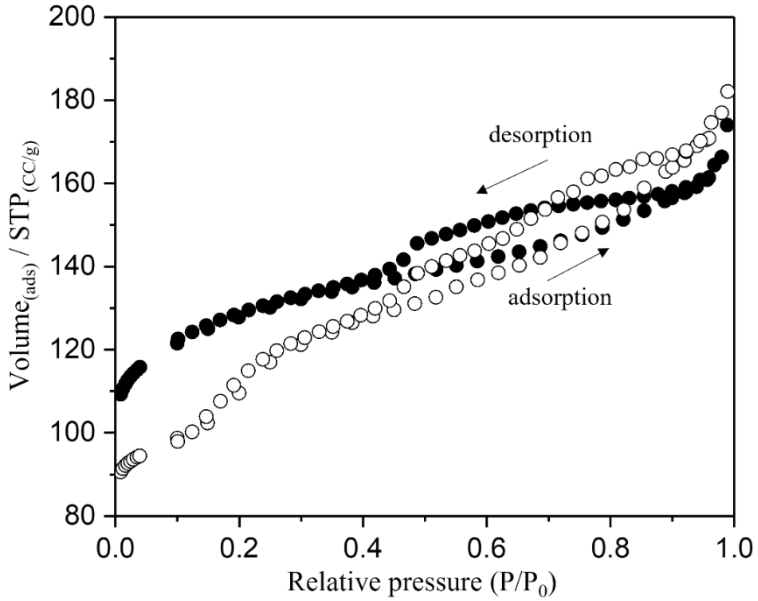

Fig. 3. N_2 adsorption and desorption isotherms of f-ZSM-5 (filled symbols) and s-ZSM-5 (open symbols).

Table 1. Physical properties of the fresh and steamed zeolites

Zeolite	$V_{(micro)}$[a] (cc/g)	$V_{(total)}$ (cc/g)	$S_{(micro)}$[a] (m^2/g)	$S_{(total)}$[b]
f-ZSM-5	0.17	0.26	347	416
s-ZSM-5	0.13	0.28	259	375

[a] t-Plot ; [b] BET method

In contrast, the isotherm of s-ZSM-5 shows a rather gradual nitrogen uptake at low relative partial pressures and the hysteresis loop extends at high relative partial pressures as compared to that of f-ZSM-5. This indicates a loss of a fraction of microporosity and a gain of a fraction of mesoporosity in s-ZSM-5. As a result, the micropore volume and surface area contribution (69%) to the total surface area decreases while, the total pore volume and mesopore surface

area increase for s-ZSM-5 as compared to that of f-ZSM-5 (Table 1). Interestingly, the total surface area of s-ZSM-5 is lower than that of f-ZSM-5. The results infer that the steam treatment of f-ZSM-5 led to formation of additional mesopores at the expense of micropores in s-ZSM-5 due to partial dislodgement of framework Al atoms [20] that might have blocked, to some degree, the micropores (Table 1). These observations are consistent with our earlier studies by solid state NMR and N_2 physisorption [20] which show a loss of micropore volume and of total surface area in ZSM-5 zeolites under mild methanol to gasoline (MTG) reaction at 623 K for 3 days. However, harsh MTG conditions (i.e., at 673 K for 3 days) led to severe steaming that resulted in a significant loss of micropore volume and of micropore surface area which favoured increased mesoporosity and total surface area [20]. The partial loss of framework Al, along with silanol groups, in s-ZSM-5 is also detected by DRIFTS (Fig. 2), as discussed above. The implications of these alterations to the ZSM-5 framework and pore architecture on the methanol adsorption capabilities of f-ZSM-5 and s-ZSM-5 are assessed by methanol adsorption isotherms collected under equilibrium at room temperature.

3.3 Methanol adsorption isotherms:

Methanol adsorption isotherms of fresh and steamed zeolites are compared in Fig. 4. Both the isotherms show a steep methanol uptake at lower pressures (p/kPa < 2) and a gradual uptake at higher pressures, which is typical for microporous materials [24,75], and is consistent with N_2 physisorption data (Fig. 3).

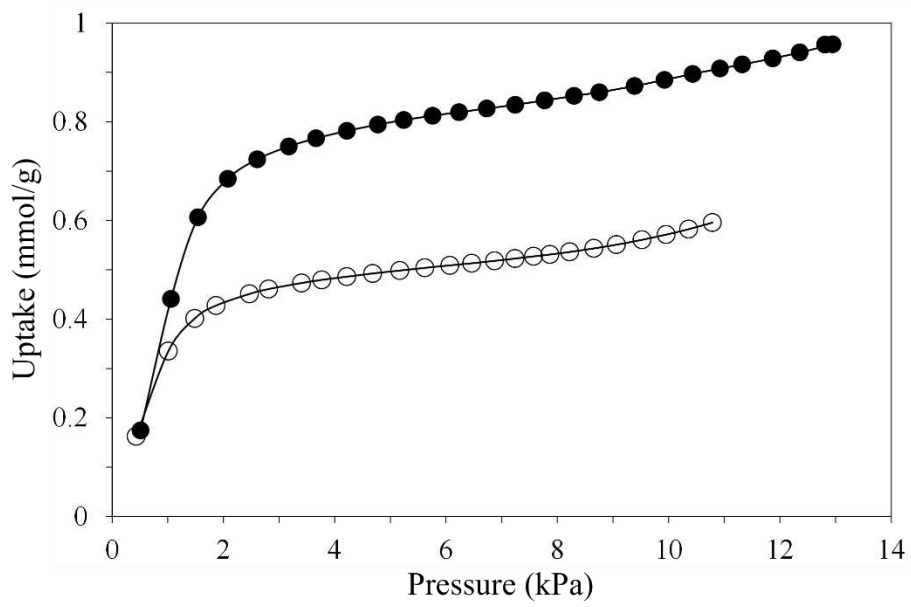

Fig. 4. Experimental methanol adsorption isotherms measured at room temperature. Fresh f-ZSM-5 (filled symbols) and steamed s-ZSM-5 (open symbols).

According to Brunauer classification, methanol isotherms of f-ZSM-5 and s-ZSM-5 can again be categorised as a type I isotherm [76]. It is evident that the absolute methanol uptake is higher in the fresh than that in the steamed zeolite over the pressure range studied. At pressures ≤ 2 kPa, the methanol uptake is ~ 78% for the fresh, while it is 67% for the steamed zeolite. It is in excellent agreement with N_2-physisorption data (Fig. 3 and Table 1) that shows a relative loss of 23% micropore volume in s-ZSM-5 as compared to f-ZSM-5. The methanol uptake for both the zeolites is more gradual at pressures above 2 kPa. The absolute methanol uptake at the maximum pressure studied is 0.90 and 0.60 mmol/g for the fresh and steamed zeolites, respectively. The amount corresponds to around 4.40 and 3.70 methanol molecules per unit cell, based on which, we suggest that ~ 1.8 and ~ 1.5 methanol molecules per acid site are adsorbed at equilibrium in f-ZSM-5 and s-ZSM-5, respectively. This indicates that the methanol adsorption capability of the steamed zeolite decreases, to some degree, which can be attributed to the loss of a fraction of easily accessible acidic hydroxyls (especially Brønsted acid sites due to dealumination, as evident from DRIFTS (Fig. 2) and the micropore data (Fig. 3) as measured by N_2-physisorption. Moreover, the absolute methanol uptake by f-ZSM-5 with Si/Al ratio of 40 is lower than that by ZSM-5 with Si/Al of 15 reported in [24] and is consistent with the acid site density of the zeolites. The higher the ratio, the lower the acid site density and hence the lower the methanol uptake by f-ZSM-5. However, the location of the methanol adsorption site within the ZSM-5 pores is unknown. Moreover, it is known to be difficult to define precisely the location of Al in ZSM-5 framework [77]. Therefore, computational tools are employed to find the potential methanol adsorption sites in ZSM-5 pores and to gain molecular insights into methanol adsorption isotherms as a function of pressure which determines the methanol loading in the zeolite pores.

3.4 Computational studies on methanol adsorption:

H-ZSM-5 models

Two models are constructed based on the Si/Al ratio (40) of the zeolite and DRIFTS data (Fig. 2) that show the presence of both Brønsted and silanol hydroxyls in the fresh and steamed zeolites. The models are depicted in Fig. 5. Two Al atoms are introduced into the unit cell of f-ZSM-5 (Fig. 5A), while only one Al atom is considered in the unit cell of s-ZSM-5 (Fig. 5B) as the steam treatment led to the partial dislodgement of framework Al as evident from DRIFTS (Fig. 2) [20]. For f-ZSM-5, the two Al atoms are placed at T8 and T10 crystallographic sites. The T10 site represents an isolated Brønsted acid site, while T8 site comprises both Brønsted

and silanol hydroxyls which are neighbouring hydroxyls. The T10 site is located within a sinusoidal channel. The T8 site is located at an intersection of straight and sinusoidal channels and, the Brønsted hydroxyl is oriented towards a sinusoidal channel while the silanol hydroxyl is positioned in a straight channel (Fig. 5A). Thus, the hydroxyls at the T8 site may not be equally accessible by methanol molecules. In addition, a silanol group is placed at the T9 site which is located at an intersection and is oriented in a straight channel. The silanols at T8 and T9 sites are created by hydrolysing [Al(T8) – O(H)] – Si – O – Si(T9) bonds and by terminating Si with OH groups such that no vacancy is left (Fig. 5A).

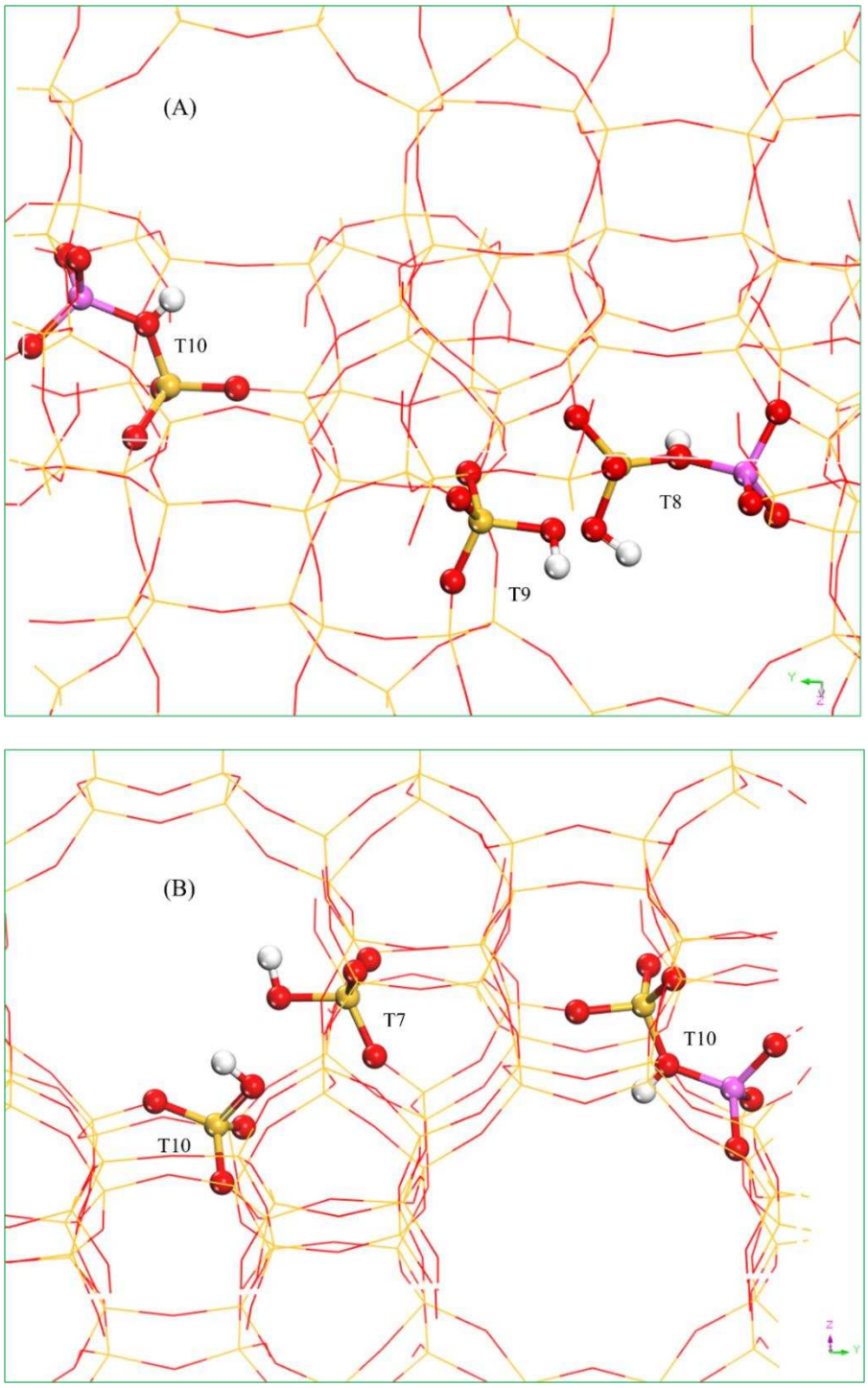

Fig. 5. Models of the fresh f-ZSM-5 (A) and steamed s-ZSM-5 (B) zeolites. The yellow, pink, red and gray denote Si, Al, O and H, respectively.

For s-ZSM-5, the Al atom is placed at the T10 site (as an isolated Brønsted acid site) which is within a sinusoidal channel, while two silanol hydroxyls are located at T10 and T7 sites. Again, the silanols at T7 and T10 sites are created by hydrolysing Si(T7) – O – Si(T10) bonds and by terminating Si with OH groups which left no vacancy (Fig. 5B). The T10 site is located within a sinusoidal channel and the T7 site is placed at an intersection and is positioned in a straight

channel (Fig. 5B). More details on the location of the T sites and the orientation of the hydroxyls are provided in Fig. S6 (SI). The selection of the T sites [77-81] for the f-ZSM-5 and s-ZSM-5 is in line with our earlier reports [17,65] that considered a more open T site either at T8 or T12 and a more confined T site either in a straight (T1, T7) or sinusoidal (T4, T7) channel [17,65] with different accessibilities and hence reactivities. Besides these models (Fig. 5), two more models, details of which are given in the SI with varied acidic hydroxyls at different crystallographic T sites (Fig. S2) are tested and found that they are inadequate to describe the experimental methanol isotherms (Fig. S7). Therefore, the discussion is limited to the models presented in Fig. 5.

3.4.1 Adsorption isotherms:

Based on the models presented in Fig. 5, methanol adsorption isotherms as a function of pressure at room temperature are generated by GCMC simulations, and the simulated isotherms of the fresh and steamed zeolites are compared with experiment in Fig. 6.

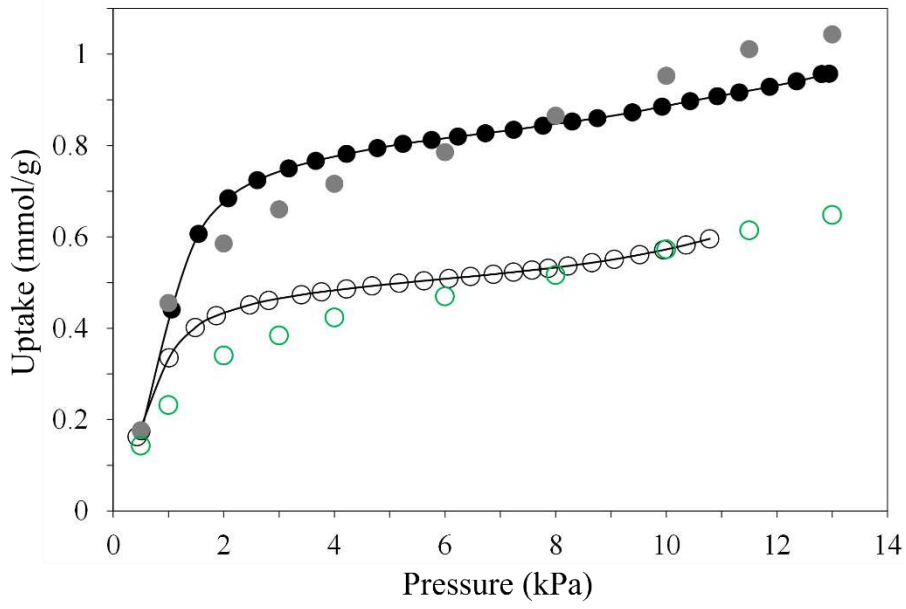

Fig. 6: Comparison of simulated with experimental methanol isotherms at room temperature. f-ZSM-5: filled symbols (Black: experimental and Grey: simulated) and s-ZSM-5 open symbols (Black: experimental and Green: simulated).

In general, the simulated isotherms match well with experiment. A closer inspection shows that the simulated methanol isotherm of f-ZSM-5 slightly underestimates the methanol uptake between 2 and 4 kPa and overestimates the uptake above 8 kPa; whereas the simulated isotherm of s-ZSM-5 underestimates, again slightly, the methanol uptake only between 1 and 4 kPa and describes the uptake very well above 8 kPa. These small variations in the simulated methanol

isotherms as compared with the experimental are to be expected because the simulations are carried out on perfect and infinite crystals, which is clearly not the case in experiment as evident from the DRIFTS (Fig. 2) and N_2 physisorption data (Fig. 3 and Table 1). The effect of acidic hydroxyls at different crystallographic sites on the nature of methanol interactions and the subsequent methanol adsorption geometry provides further insight into the methanol adsorption isotherms. Therefore, the configurations generated in the GCMC simulations are considered in more detail below.

3.4.2 Sorbate structures in different pressure regions:

In the pressure range used to simulate methanol adsorption isotherms in Fig. 6, we focus on data collected at 0.4 and ≥10 kPa which represent the lowest and highest methanol uptake, respectively. These data are of particular interest in assessing the nature of the methanol interactions with acidic hydroxyls and adsorption geometry as a function of methanol loading; and we recall that the reactivity of methanol in H-ZSM-5 with Si/Al of 25 and 30 is methanol loading dependent at room temperature [12,13,17]. The configurations generated by GCMC simulations at 0.4 kPa and ≥10 kPa are depicted in Figs. 7 and 8. Refinement of these and other configurations using the DFT methodologies will be reported later (Fig. 9 and 10).

The methanol adsorption capacity of 2 molecules per unit cell at 0.4 kPa and 4 molecules per unit cell at 12.5 kPa is derived by GCMC simulations for the fresh zeolite (Fig. 7). We note that the change in the geometry of the ZSM-5 framework is negligible upon methanol adsorption at these pressures and therefore the geometry of the ZSM-5 framework is considered stable for GCMC simulations. The adsorption capacity corresponds to 1 and ~ 2 methanol molecules per Brønsted hydroxyl, respectively, in excellent agreement with the experimental data as discussed in Section 3.3. The simulations show that the methanol molecules are predominantly distributed around Brønsted acidic hydroxyls. At 0.4 kPa, where the lowest methanol uptake is measured and simulated (Fig. 6), one methanol molecule interacts with the isolated Brønsted acidic hydroxyl at the T10 site of the sinusoidal channel, and the other methanol molecule interacts with silanol hydroxyl at the T8 site, which neighbours a Brønsted acidic hydroxyl at the same site that is oriented in the sinusoidal channel. Interestingly, no methanol molecule interacts with

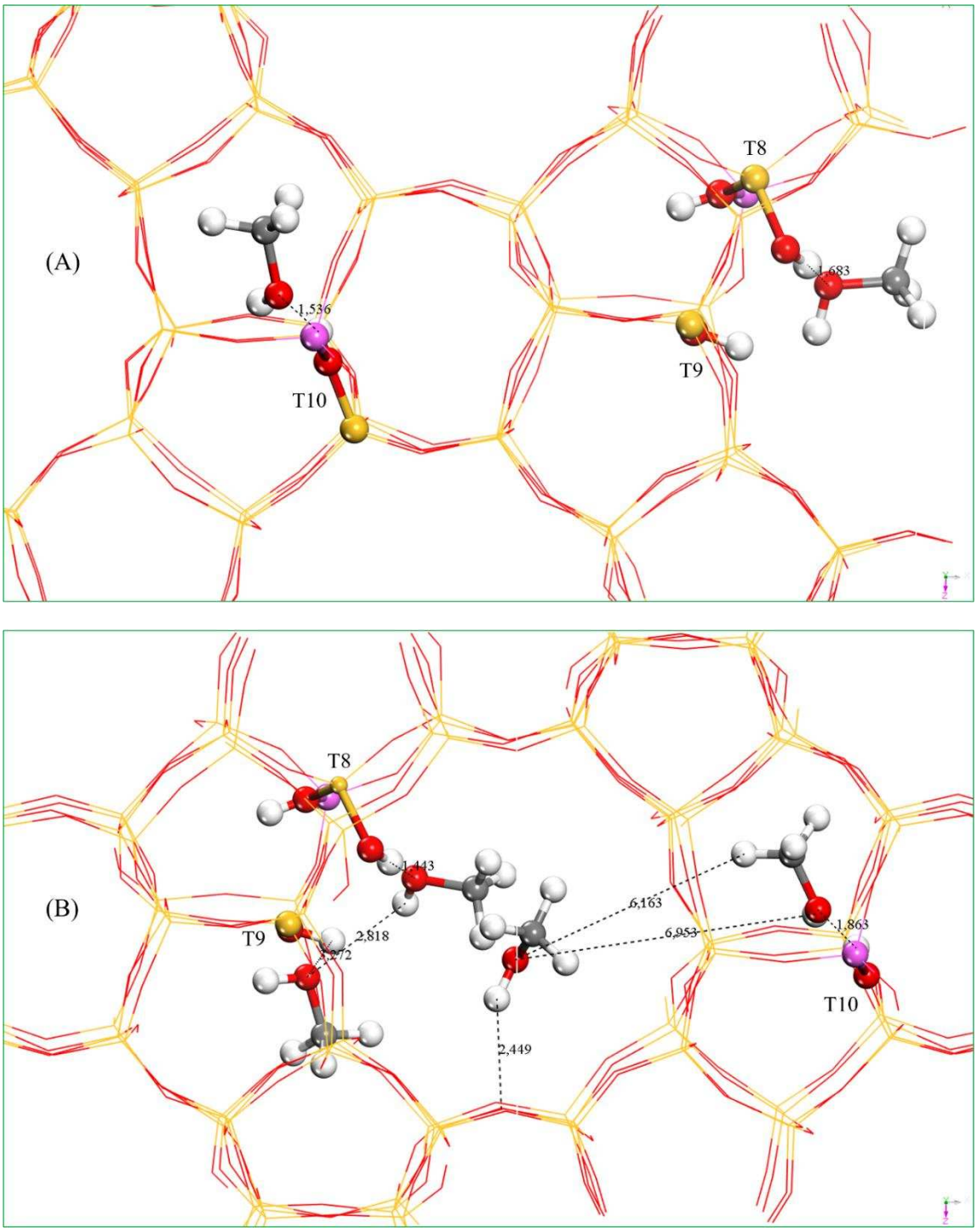

Fig. 7: Methanol adsorption geometry in f-ZSM-5 at 0.4 kPa (A) and 12.5 kPa (B).

the isolated silanol hydroxyls at the T9 site even though it is positioned in the straight channel. These observations suggest that the nature of hydroxyl groups determines their reactivity towards methanol, which is in line with work that reports cooperative effects of neighbouring Brønsted hydroxyls that significantly reduce the energy barrier for methanol reactivity compared with the isolated Brønsted site [17]. Similarly, the observed differences in the reactivity of silanol hydroxyls at T8 and T9 sites towards methanol adsorption can be attributed

to the cooperative effects of neighbouring Brønsted and silanol hydroxyls at the T8 site. Moreover, the silanol hydroxyl at the T8 site appears to be preferred over the Brønsted hydroxyl for the methanol adsorption, which could be attributed to the accessibility of the sites. The methanol adsorption geometry at the T10 site indicates interactions between O of the methanol molecule and the H of the Brønsted acidic hydroxyl of the T10 site giving rise to the end-on configuration with an interaction distance of around 1.536 Å, which is typical of a hydrogen bond with strong interactions [17,65]. Whereas, the methanol adsorption geometry at the T8 site suggests interactions between O of the methanol molecule and the H of the silanol group of the T8 site with the side-on configuration [17,65] and an interaction distance of around 1.683 Å, indicating that the interaction is somewhat weaker than that at the T10 site.

At 12.5 kPa, where the highest methanol uptake is observed (Fig. 6), two methanol molecules interact with the Brønsted acidic hydroxyl at the T10 site, and two more interact with the silanol group at the T8 site that neighbours a Brønsted acidic hydroxyl, which suggests that the methanol molecules cluster around acidic hydroxyls at higher pressures, unlike at lower pressures. Interestingly, no methanol molecule interacts directly with the isolated silanol group at the T9 site which, however, appears to interact weakly with a second methanol molecule of the cluster at the T8 site (Fig. 7B). The methanol adsorption geometry at the T10 site appears to be an end-on configuration with an interaction distance between the methanol molecule and acidic site of around 1.863 Å, while the geometry at the T8 site appears to be a side-on configuration with an interaction distance of around 1.443 Å. Note that the distance between the O of methanol and the T10 site is higher at 12.5 kPa than at 0.4 kPa, probably due to the lateral interactions between the clustered methanol molecules. Also, the distance between the methanol molecule and adsorption site at T10 (1.863 Å) is larger than that at the T8 site (1.443 Å), suggesting that the interactions are stronger in the straight channel than those in the sinusoidal, which in turn could be due to the effect of steric hindrances at higher methanol pressures that may be better accommodated in the straight rather than in the sinusoidal channels. This observation could also explain the anomalous distance (6.1 and 6.9 Å) between the two clustered methanol molecules at the T10 site. The interaction distance between the clustered molecules at the T10 site is still shorter than that between the second methanol of the cluster at the T10 site and the cluster at the T8 site. Note that the GCMC simulations capture only a possible thermodynamic equilibrium state and do not include kinetic effects, unlike molecular dynamics (MD) simulations. [17].

For the steamed zeolite, the methanol adsorption capacity of 2 molecules per unit cell at 0.4 kPa and 3 molecules per unit cell at 10 kPa is determined by GCMC simulations, in agreement

with the experimental data as discussed in Section 3.3. The simulations show that methanol molecules also preferentially adsorb on Brønsted acidic hydroxyls in the steamed zeolite s-ZSM-5 as in f-ZSM-5 (Fig. 8). Interestingly, two methanol molecules interact with the T10 site (Brønsted hydroxyl) at 0.4 kPa and 10 kPa, unlike in the fresh f-ZSM-5 (Fig. 7).

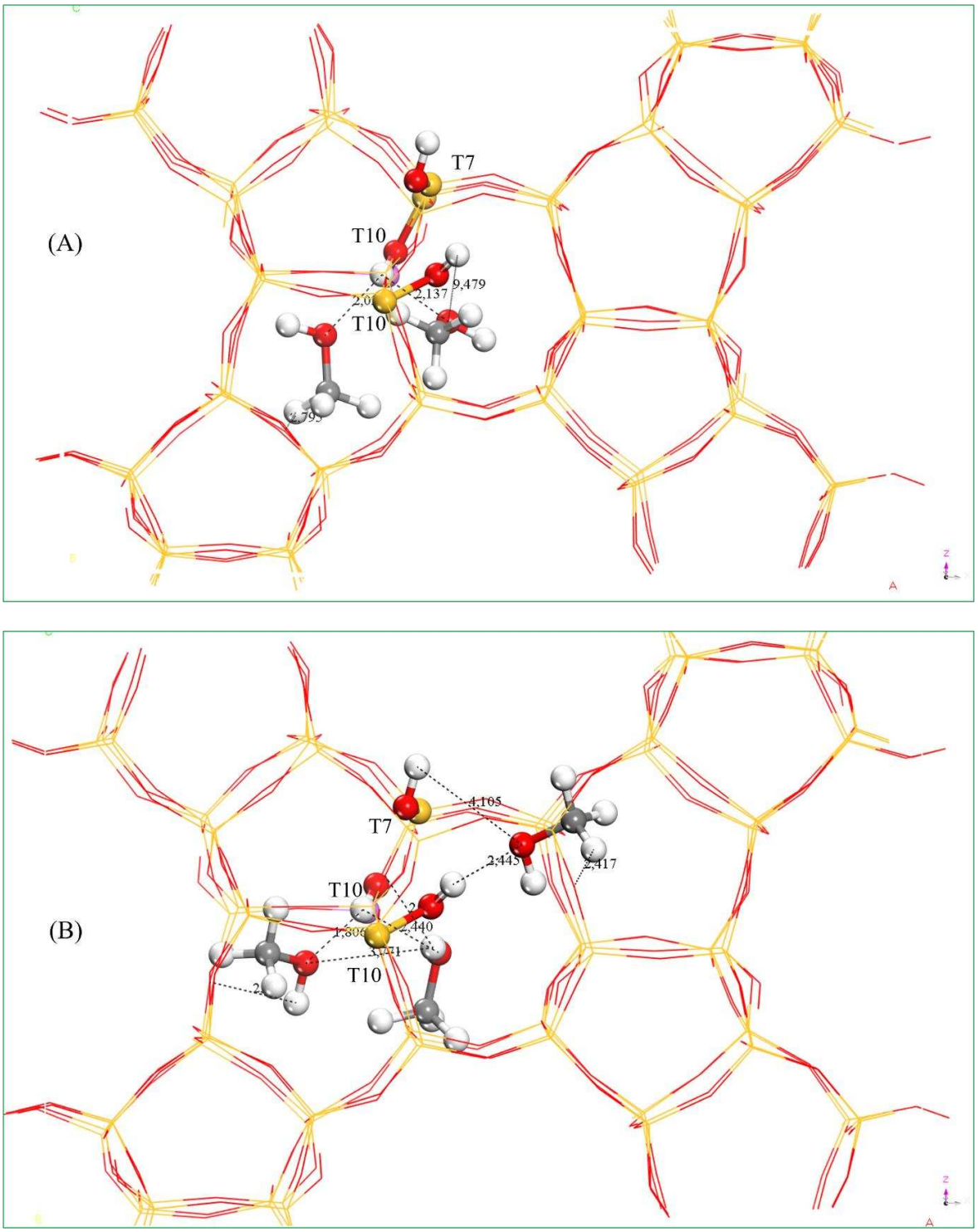

Fig. 8. Methanol adsorption geometry in s-ZSM-5 at 0.4 kPa (A) and 10 kPa (B).

Significantly, no methanol molecules interact with the isolated silanol groups of T7 and T10 sites at 0.4 kPa and, only one methanol molecule is adsorbed on the T10 site at 10 kPa. It is noteworthy that the methanol molecules cluster around the T10 Brønsted hydroxyl site of s-ZSM-5 either at 0.4 kPa or 10 kPa, which is in a marked contrast to the fresh zeolite (Fig. 7), which implies that the Brønsted acidic hydroxyls are more reactive than the silanol groups. The interactions between methanol molecules and the T10 (Brønsted) site exhibit two configurations. At 0.4 kPa: i) the end-on configuration with an interaction distance of around 2.01 Å and ii) side-on configuration with 2.137 Å (Fig. 8A), and at 10 kPa: i) side-on configuration with interaction distances of 1.806 Å and ii) end-on configuration with an interaction distance of 2.44 Å (Fig. 8B). The adsorption geometry of the methanol molecule on the T10 silanol site at 10 kPa is the side-on configuration with an interaction distance of around 2.445Å.

Clearly methanol molecules preferentially interact with Brønsted acidic hydroxyls, but also with silanol groups neighbouring the Brønsted hydroxyls rather than isolated silanol groups (Fig. 7A and Fig. 8A). Moreover, interactions between methanol molecules and Brønsted acidic hydroxyls (either isolated or neighbouring silanols) are stronger than those between methanol molecules and isolated silanol groups as evident from the interaction distances between the molecules and adsorption sites. The preferential methanol interaction with the Brønsted acidic sites is in line with dealumination that decreases the number of Brønsted acidic sites (Fig. 2) and hence the absolute methanol uptake as evident from Fig. 6. The preferential methanol interactions are further assessed by the electrostatic interactions, which contribute to the interatomic potential energy, between acidic hydroxyls of both Brønsted and silanol groups and methanol molecules. The electrostatic contribution to the potential energy is accounted by assigning partial charges to all atoms of the fresh and steamed zeolite structures. The partial charges determined by DDEC6 approach are listed in (Table 2) and the corresponding structures are depicted in Fig. S3 and Fig. S4.

Table 2. The partial charges of the fresh and steamed zeolites.

Atoms	Label	Charge (e-) calculated by DDEC6
f-ZSM-5		
O	O	-0.9626
Al	Al	1.8463
Si	Si	1.9133

H	H[a]	0.5148
H	H[b]	0.3987
O	O[a]	-0.8699
O	O[b]	-0.8238
s-ZSM-5		
O	O	-0.9603
Al	Al	1.8466
Si	Si	1.9143
H	H[a]	0.5158
H	H[b]	0.3886
O	O[a]	-0.9111
O	O[b]	-0.8165

[a] Brønsted acidic site; [b] Silanol groups

It is evident that the partial charges of O and H atoms of the Brønsted hydroxyls are always higher than the silanol groups in both fresh and steamed zeolite models, consistent with the reactivity of the hydroxyls towards methanol molecules [6,12,13].

The reactivity of acidic hydroxyls of fresh and steamed zeolites towards methanol is corroborated by the methanol adsorption enthalpies. For this, adsorption enthalpies are calculated for one methanol molecule per unit cell in the same zeolite models depicted in Fig. 5 by GCMC simulations (described in Section 2.5). Although one molecule per unit cell is a lower methanol loading than that studied for the methanol adsorption isotherms (Fig. 4 and Fig. 6), if we wish to evaluate the interaction of single methanol molecules with the acid site and we must eliminate methanol cluster formation. As the cluster formation can potentially affect the adsorption enthalpies by intermolecular interactions of methanol molecules. The resulting methanol adsorption (at T10 site as side on configuration) enthalpies for the fresh and steamed zeolites are -48 and -34 kJ/mol, respectively. The difference in the adsorption enthalpies between the two zeolites indicates that the interactions between methanol molecule and the Brønsted acidic hydroxyl are stronger in f-ZSM-5 than that in s-ZSM-5 (Fig. S8). These observations are in general consistent with DFT *based* calculations [65,66] and experimental values of similar zeolites [24,82]. The earlier DFT based calculations show that the enthalpies of methanol adsorption at T1, T4 and T12 sites of ZSM-5 are in the range of -84 to -98, -18 to -30 and -50 to -69 kJ/mol, respectively [66]. Another study using DFT with B97-3 show

adsorption enthalpies of methanol with a side on configuration (similar to the present work) at T1, T4 and T12 of -85, -80 and -78 kJ/mol, respectively [65]. These values differed when enthalpies are calculated using DFT with either B97-D or MP2 [65], suggesting the sensitivity of adsorption energies to the DFT method employed. It also appears from the earlier DFT and the present GCMC calculations that the adsorption enthalpies depend on the nature and location of the T site. Therefore, the adsorption energies and geometries are further refined by more advanced periodic DFT with PBE and QM/MM calculations, with the results summarised in Table 3 and Fig. 9.

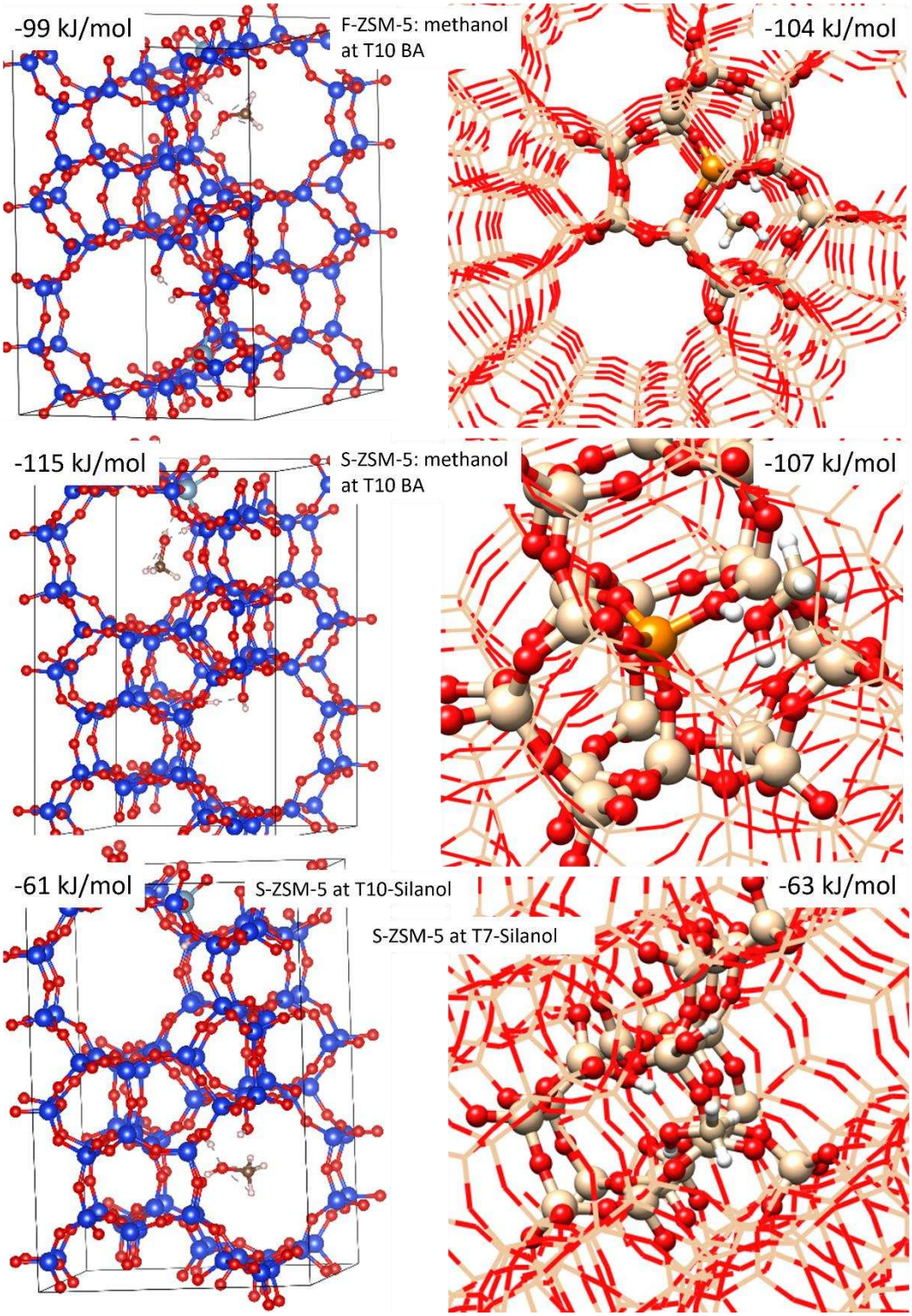

Fig. 9. Methanol adsorption energies and geometries for one methanol molecule per unit cell are calculated by DFT with PBE (left) and QM/MM (right) and the corresponding methanol configurations at Brønsted hydroxyl at T10 (f-ZSM-5 and s-ZSM-5) and silanols at T10 and T7 (s-ZSM-5). Colour scheme: (left) blue, light blue, red and gray denote Si, Al, O and H; (right) brown, yellow, red and gray denote Si, Al, O and H, respectively.

The periodic DFT and QM/MM calculations of a single methanol adsorption at the T10 Brønsted hydroxyl in both f-ZSM-5 and s-ZSM-5 show comparable adsorption energies (Fig.

9 and Table 3). The calculated bond distance between the T10 Brønsted acidic proton and the methanol oxygen are as follows: 1.68Å in the case of a single molecule of methanol in F-ZSM-5 and 1.43Å for S-ZSM-5, when calculated at DFT/PBE level of theory. This value changed slightly to 1.42Å in the case of a single molecule of methanol in F-ZSM-5 and 1.60Å for S-ZSM-5, when calculated using QM/MM methodology. The major change occurred when comparing the binding of two molecules of methanol to the T10 site of S-ZSM-5 at different levels of theory; where a large decrease in Brønsted acidic site methanol bond distance was observed in the case of the QM/MM model (1.04Å) over the DFT/PBE model 1.43Å. This large decrease in bond distance is caused by the barrierless transfer of the Brønsted acidic site proton to the methanol in the latter.

Table 3. Calculated methanol adsorption energies in ZSM-5 by using different theoretical approaches.

ZSM-5	Methano load[a]	T site	Energy (kJ/mol)	Theory	Reference
Fresh	1	10	-48	GCMC	Present work
			-99	DFT PBE	
			-107	QM/MM	
	1	12	-186.8	PW91	66[d]
			-177.5	B3LYP	
			-168.9	B97-2	
	1	1	-85	DFT B97-3	65[d]
		4	-80		
		12	-78		
	1	1	-113	DFT MP2	
		4	-112		
		12	-113		
	2	8[b]	-180	DFT PBE	Present work
			-116	QM/MM	
	2	12	-98 to -146	DFT B97-3	65[e]
Steamed	1	10	-34	GCMC	Present work
			-115	DFT PBE	
			-107	QM/MM	

		10[b]	-61	DFT PBE	
		7[c]	-63	QM/MM	
	2	10	-155	DFT PBE	Present work
			-199	QM/MM	

[a] Methanol molecules per hydroxyl; [b] T8 Brønsted hydroxyl neighbouring theT9 silanol site; [c] Silanol group; [d] side on methanol adsorption configuration and [e] different adsorption geometries (mono, bi and tridentate)

The adsorption energies calculated by periodic DFT with PBE are -99 and -115 kJ/mol for the fresh and steamed zeolite, respectively. QM/MM calculations show -104 kJ/mol for the fresh zeolite and -107 kJ/mol for the steamed. The adsorption energies calculated by periodic DFT and QM/MM are much higher than those obtained by GCMC calculations for the same T site and with the same methanol loading. Also, these adsorption energies are higher than those reported by DFT with different levels of theory including B97-3, B97-D or MP2 (Table 3), confirming the complexity associated with the methanol adsorption energy calculations. Interestingly, adsorption energies calculated for methanol at T10 and T7 silanol sites of steamed s-ZSM-5 are ~ 60 kJ/mol (Fig. 9 and Table 3) which is significantly lower than that calculated for methanol at a Brønsted acid site and is consistent with the reactivity of the hydroxyls towards methanol as noted above [6,12,13].

Taking advantage of the periodic DFT and QM/MM calculations as compared to GCMC, the methanol loading per hydroxyl is increased from one to two molecules (Fig. 10 and Table 3). The loading represents the methanol adsorption isotherms with an adsorption capacity of ~ 2 methanol molecules per Brønsted hydroxyl at 12.5 kPa (Figs. 4 and 6) and enables the assessment of adsorption energies as a function of methanol loading. Adsorption energies of methanol at T8 Brønsted hydroxyl that neighbours T9 silanol site in f-ZSM-5 are calculated to be -180 and -116 kJ/mol by DFT and QM/MM, respectively (Fig. 10 and Table 3). The adsorption energies are higher than those calculated for one methanol molecule per hydroxyl (Fig. 9 and Table 3), though the T sites employed are different. Interestingly, the steamed s-ZSM-5 with two methanol molecules at T10 Brønsted site, which is similar to the site employed for one methanol molecule per acidic hydroxyl (Fig. 9), results in adsorption energies of -155 by DFT and -199 kJ/mol by QM/MM. We note that periodic DFT finds a stable minimum for the methanol dimer and protonated T10 Brønsted hydroxyl while QM/MM shows a barrierless proton transfer from the Brønsted hydroxyl to the proximal methanol dimer. Despite repeated attempts to scan this proton back to its original T10 site position as with the periodic

calculations, no stable minimum was found and therefore the adsorption energy of this protonated methanol complex (methyl oxonium) is considerably higher at −199 kJ/mol (Fig. 10). These observations confirm that the adsorption energies are sensitive to methanol loading (Table 3). Based on the present and earlier calculations [17,24,65,66,82], it is evident that the methanol adsorption energies are dependent on various factors including the nature and the location of the hydroxyls as well as the number of methanol molecules per hydroxyl. Therefore, direct comparison between the calculations and experimental data can be a challenging task as experimental data may represent an average value of all the factors that contribute to the methanol adsorption. Methanol adsorption energies calculated with DFT at ≥10 kPa obtained values of -84 kJ/mol per methanol molecule for the f-ZSM-5 unit cell, which is considerably higher than the -76 kJ/mol per methanol molecule for the s-ZSM-5 unit cell, with the former averaging an additional methanol molecule adsorption per unit cell (Fig. S9). . Very similar methanol adsorption geometries were observed when comparing the periodic DFT and GCMC ionic potential methods; however, considerable difference were seen when comparing these geometries to those obtained with the QM/MM cluster approach, which is most evident when the dimer configuration is calculated at the T10 acid site of s-ZSM-5 (see Fig. 10), here the higher level of DFT used in the QM/MM approach leads to a barrierless transfer of the acid site proton to the proximal methanol.

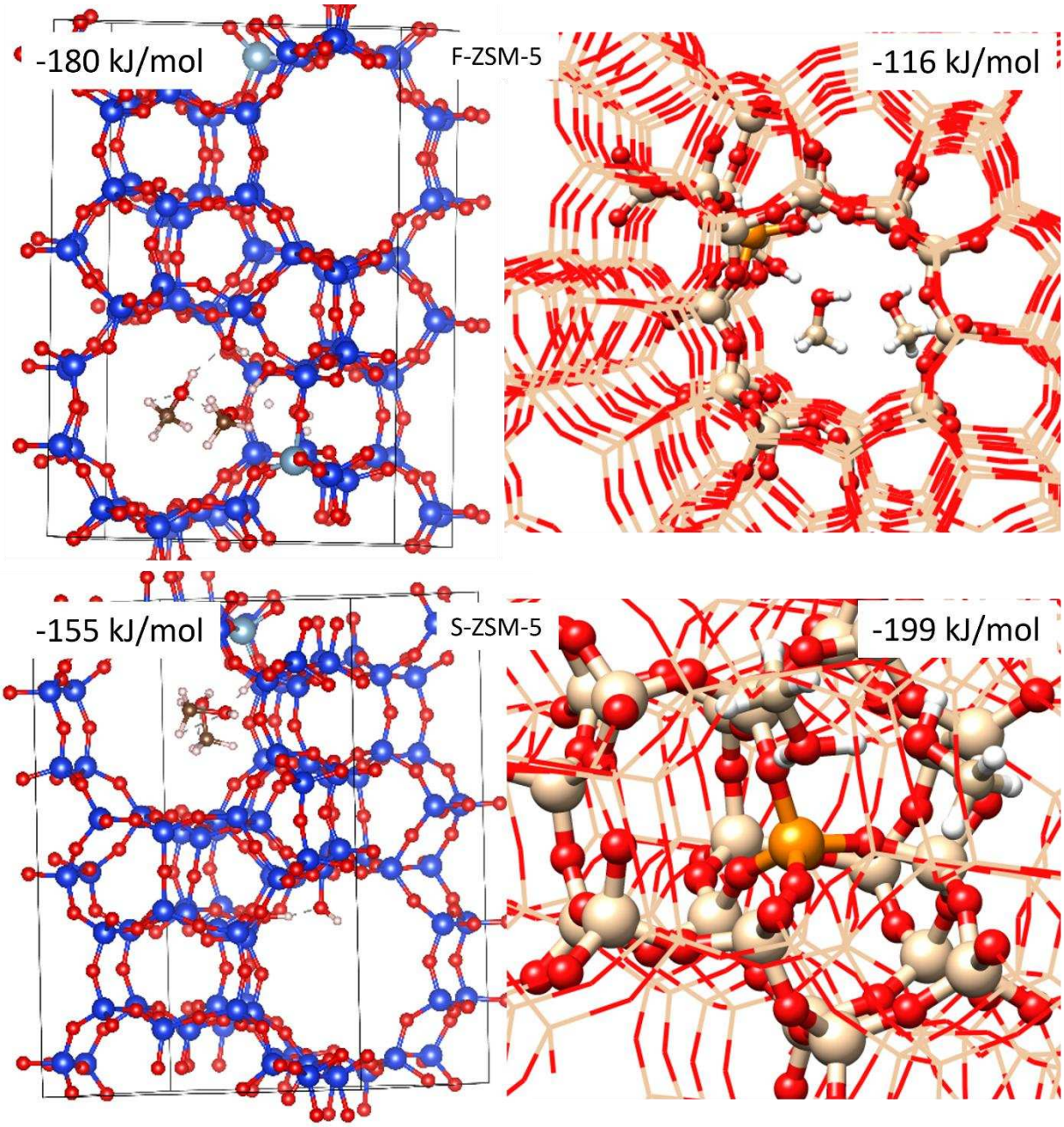

Fig. 10. Methanol adsorption energies for two methanol molecules per unit cell are calculated by periodic DFT with PBE (left) and QM/MM (right) and the corresponding methanol adsorption configurations at T8 Brønsted hydroxyl that neighbours T9 silanol site in f-ZSM-5 and T10 Brønsted hydroxyl in s-ZSM-5. Colour scheme: (left) blue, yellow, red and gray denote Si, Al, O and H, (right) brown, yellow, red and gray denote Si, Al, O and H, respectively.

The calorimetric experiments at 50 °C yield two different methanol adsorption enthalpies of -47 and -74 kJ/mol for the same H-ZSM-5 with Si/Al ratio of 36 [82]. Similarly, desorption enthalpies of methanol on H-ZSM-5 (Si/Al ~ 38) are 47 and 74 kJ/mol as derived by the TDP desorption experiments. In the above two studies [24,82], the different adsorption and desorption enthalpies were attributed to the heterogeneous surface site energies of the zeolite modifying the nature of interactions. The experimental values fall, not surprisingly, between

the enthalpy values derived by GCMC and, periodic DFT and QM/MM calculations for one methanol molecule per unit cell. The results are consistent with our earlier operando DRIFTS/mass spectrometric studies (at room temperature), on fresh H-ZSM-5 with Si/Al of 25 and 30, which show that Brønsted acidic hydroxyls are more reactive towards methanol than to silanol groups [12,13]. At a methanol loading of ≤1 molecule per acidic site, which is similar to the methanol loading at 0.4 kPa (Fig. 5 and Fig. 6), the methanol preferentially adsorbed at Brønsted acidic hydroxyls with a neutral structure, and silanol groups are largely inactive in the methanol adsorption process. In contrast, methanol adsorbed on Brønsted and silanol hydroxyls at a methanol loading of ≥2 molecules per acidic site, which is comparable to methanol loading at >10 kPa in Fig. 5 and Fig. 6, are clustered at acidic sites with a protonated structure [6,10,12,13]. These experimental observations are also corroborated by our periodic DFT and QM/MM calculations, and the first-principles MD simulations [17,65].

Based on the above analyses, it can be suggested that the nature and location of acidic hydroxyls play a critical role in the methanol adsorption process which is also affected by the simultaneous presence of different acidic hydroxyls as evident by methanol adsorption at T8 Brønsted acid site that neighbours T9 silanol site as reported in Fig. 10 [17]. At the highest methanol uptake, methanol molecules tend to form clusters around T10 and T8 sites of f-ZSM-5 (Fig. 7), consistent with periodic DFT and QM/MM calculations (Fig. 10). There is also a clear indication that the location of the silanol groups affects the formation of the methanol clusters. The silanol hydroxyl at the T8 site that neighbours a Brønsted acidic hydroxyl at the same crystallographic site favours the formation of methanol cluster more than that at the T9 site of an isolated silanol group which is located at an intersection and is oriented in a straight channel. Moreover, isolated silanol groups at T7 of s-ZSM-5 and T9 of f-ZSM-5 (located at an intersection and oriented in a straight channel, see Fig. 7B and 8B) are inactive under these conditions, while the T10 site (isolated silanol group) of s-ZSM-5 interacts with one methanol molecule only at higher pressures (Fig. 8B), which suggests that the location of silanol hydroxyls determines its activity towards methanol. The significance of the nature, location and distribution of acidic hydroxyls on the methanol adsorption profiles is confirmed by simulating methanol adsorption isotherms using different crystallographic sites (Fig. S2) than those reported in Fig. 5, and it is evident from Fig. S7 that the simulated methanol isotherms could not describe the experimental. Based on this, it can be suggested that the methanol adsorption isotherms and subsequent GCMC simulations provide a means to identify adsorption sites and hence to define deactivation caused by dealumination of ZSM-5 in methanol conversion such as MTH. The same method can potentially also shed light on the discrepancies observed on the

surface adsorbed species over different ZSM-5 (with comparable Si/Al ratios) samples that may either originate from different synthesis batches or from sources/suppliers [12,13].

4. Summary and Conclusions

Methanol adsorption isotherms of zeolites ZSM-5 are studied by experiment and Grand Canonical Monte Carlo (GCMC) simulations with the aim of understanding the methanol adsorption capacity, geometry and sites as a function of steam treatment (at 573 K for 24h).. The fresh (f-ZSM-5) and steamed (s-ZSM-5) zeolites are characterised by diffuse reflectance infrared Fourier transformed spectroscopy (DRIFTS) and N_2-physisorption. DRIFTS shows the presence of both Brønsted and silanol hydroxyls in f-ZSM-5 and the concentration of these hydroxyl groups, especially the Brønsted acid species, decreases considerably upon steam treatment (at 573 K for 24) in s-ZSM-5 due to dealumination. In line with this observation N_2-physisorption reveals that the total surface area (416 m^2/g) of the fresh zeolite is mainly due to micropores. The contribution of micropores decreases while that of mesopores increases as a proportion of the total surface area of the steamed zeolite. Even though the mesopores contribution increases in the steamed zeolite, the total surface area (375 m^2/g) is lower than the fresh zeolite due to pore plugging caused by partial dislodgement of framework Al on steam treatment. Implications of the steam treatment on the methanol adsorption capacity of the zeolites are evident from experimental methanol adsorption isotherms (collected at room temperature under equilibrium) and GCMC simulations. Based on this, the following main conclusions can be drawn:

1. The overall methanol uptake is higher (in the studied pressure range between 0 and ≥10 kPa) for the fresh than that for the steamed zeolite, in line with the Brønsted acid site density as evident by DRIFTS.
2. GCMC simulations reveal that the nature, location and distribution of acidic hydroxyls determine the methanol adsorption capacity, geometry and hence profiles of f-ZSM-5 and s-ZSM-5. Accordingly, simulations predict an altered nature and distribution of acidic hydroxyls in s-ZSM-5 as compared in f-ZSM-5. The former exhibits hydroxyls at T7 (isolated silanol), T10 (isolated silanol) and T10 (isolated Brønsted), while the latter shows at T8 (neighbouring silanol and Brønsted), T9 (isolated silanol) and T10 (isolated Brønsted).
3. Methanol molecules are mainly distributed, within the studied loading between one (lowest) and two (highest) molecules per Brønsted site, around Brønsted hydroxyls which are more reactive than the silanol groups. In f-ZSM-5, the silanol hydroxyl that

neighbours a Brønsted hydroxyl is more reactive than the isolated silanol groups due to the cooperative effects of the neighbouring hydroxyls. Such neighbouring hydroxyls are not predicted by GCMC in s-ZSM-5. Among the isolated silanol hydroxyls, T10 is more reactive than the T7 and T9 sites.

4. The methanol adsorption geometry on the Brønsted hydroxyls is an end-on configuration while it is a side-on configuration on silanol. The methanol adsorption energies calculated by GCMC, periodic DFT and QM/MM show that the energies are sensitive to the T site and methanol loading.

Finally, it can be suggested that the combination of methanol adsorption isotherms and GCMC simulations enables to identify sites that are responsible for activity, deactivation by dealumination and sorption/separation capabilities of zeolite ZSM-5.

Conflicts of interest

There are no conflicts of interest to declare.

Acknowledgements:

The UK Catalysis Hub is thanked for resources and support provided via our membership of the UK Catalysis Hub Consortium and funded by EPSRC grant: EP/R026939/1, EP/ R026815/1, EP/R026645/1, EP/R027129/1. GCMC calculations were carried out using Computational Chemistry HPC facility at University College London. Computing facilities for this work were provided by ARCCA at Cardiff University, HPC Wales, and the UK national HPC facility, ARCHER2 (http://www.archer2.ac.uk), through our membership of the U.K.'s Materials Chemistry Consortium (MCC) which is funded by EPSRC (EP/X035859). This work also used the Cirrus UK National Tier-2HPC Service at EPCC (http://www.cirrus.ac.uk) funded by the University of Edinburgh and EPSRC (EP/P020267/1).

5. References

[1] C. D. Chang, A. J. Silvestri, J. Catal. 47 (1977) 249-259. https://doi.org/10.1016/0021-9517(77)90172-5

[2] L. Palumbo, F. Bonino, P. Beato, M. Bjørgen, A. Zecchina, S. Bordiga, J. Phys. Chem. C 112 (2008) 9710–9716. https://doi.org/10.1021/jp800762v

[3] V. Van Speybroeck, K. Hemelsoet, L. Joos, M. Waroquier, R. G. Bell, C. R. A. Catlow, Chem. Soc. Rev. 44 (2015) 7044–7111. https://doi.org/10.1039/c5cs00029g

[4] U. Olsbye, S. Svelle, K. P. Lillerud, Z. H. Wei, Y. Y. Chen, J. F. Li, J. G. Wang, W. B. Fan, Chem. Soc. Rev. 44 (2015) 7155–7176. https://doi.org/10.1039/c5cs00304k

[5] Y. Ono, T. Mori, J. Chem. Soc. Faraday Trans. 1, 77 (1981) 2209–2221. https://doi.org/10.1039/F19817702209

[6] A. Zecchina, S. Bordiga, G. Spoto, D. Scarano, G. Spanò, F. Geobaldo, J. Chem. Soc. Faraday Trans. 92(23) (1996) 4863–4875. https://doi.org/10.1039/FT9969204863.

[7] P. E. Sinclair, C. R. A. Catlow, J. Chem. Soc. Faraday Trans. 92 (1996) 2099–2105. https://doi.org/10.1039/FT9969202099

[8] P. E. Sinclair, C. R. A. Catlow, J. Chem. Soc. Faraday Trans. 93 (1997) 333–345. https://doi.org/10.1039/A606198B

[9] W. Wang, A. Buchholz, M. Seiler, and M. Hunger, J. Am. Chem. Soc. 125 (2003) 15260–15267, https://doi.org/10.1021/ja0304244

[10] B. T. L. Bleken, L. Mino, F. Giordanino, P. Beato, S. Svelle, K. P. Lilleruda,S. Bordiga, Phys. Chem. Chem. Phys. 15 (2013) 13363–13370. https://doi.org/10.1039/c3cp51280k

[11] A. J. O'Malley, S. F. Parker, A. Chutia, M. R. Farrow, I. P. Silverwood, V. García-Sakaic, C. R. A. Catlow, Chem. Commun. 52 (2016) 2897–2900, https://doi.org/10.1039/c5cc08956e

[12] S. K. Matam, R. F. Howe, A. Thetford, C. R. A. Catlow, Chem. Commun. 54 (2018) 12875–12878. https://doi.org/10.1039/C8CC07444E

[13] S. K. Matam, S. A. F. Nastase, A. J. Logsdail, C. Richard. A Catlow, Chem. Sci.11 (2020) 6805–6814. https://doi.org/10.1039/d0sc01924k

[14] S. R. Blaszkowski, R. A. Van Santen. J. Phys. Chem. B 101 (1997) 2292–2305. https://doi.org/10.1021/jp962006+

[15] E. Sandre, M. C. Payne, J. D. Gale, Chem. Commun. (1998) 2445–2446. https://doi.org/10.1039/a806437g

[16] D. Lesthaeghe, V. Van Speybroeck, G. B. Marin, M. Waroquier, Angew. Chemie - Int. Ed. 45 (2006) 1714–1719. https://doi.org/10.1002/anie.200503824

[17] S. A. F. Nastase, P. Cnudde, L. Vanduyfhuys, K. De Wispelaere, V. Van Speybroeck, C. Richard A. Catlow, Andrew J. Logsdail, ACS Catal. 10 (2020) 8904–8915. https://doi.org/10.1021/acscatal.0c01454.

[18] S. Mitra, V. S. Kamble, A. K. Tripathi, N. M. Gupta, R. Mukhopadhyay, Pramana - J. Phys. 63 (2004) 443–448.

[19] N. M. Gupta, D. Kumar, V. S. Kamble, S. Mitra, R. Mukhopadhyay, V. B. Kartha, J. Phys. Chem. B 110 (2006) 4815–4823. https://doi.org/10.1021/jp053668e

[20] S. K. Matam, A. J. O'Malley, C. R. A. Catlow, Suwardiyanto, P. Collier, A. P. Hawkins, A. Zachariou, D. Lennon, I. Silverwood, S. F. Parker, R. F. Howe, Catal. Sci. Technol. 8 (2018) 3304–3312. https://doi.org/10.1039/c8cy00422f

[21] S. K. Matam, C. R. A. Catlow, I. P. Silverwood, A. J. O'Malley, Top. Catal. 64 (2021) 699–706. https://doi.org/10.1007/s11244-021-01450-z

[22] H. Jobic, A. Renouprez, M. Bee, C. Poinsignon, J. Phys. Chem. 90 (1986) 1059–1065, https://doi.org/10.1021/j100278a020

[23] T. Allen, Gas adsorption. In: Particle size measurement. Powder Technology. Springer, Dordrecht (1990). https://doi.org/10.1007/978-94-009-0417-0_16

[24] B. Hunger, S. Matysik, M. Heuchel, W. D. Einicke, Langmuir, 13 (1997) 6249–6254. https://doi.org/10.1021/la970615i

[25] G. Mirth, J. A. Lercher, M. W. Anderson, J. Klinowski, J. Chem. Soc. Faraday Trans. 86 (1990) 3039–3044. https://doi.org/10.1039/FT9908603039

[26] K. Heijmans, I. C. Tranca, M. W. Chang, T. J. H. Vlugt, S. V. Gaastra-Nedea, D. M. J. Smeulders, ACS Omega, 6 (2021) 32475–32484, https://doi.org/10.1021/acsomega.1c03909

[27] R. Catlow, R. Bell, F. Corà, B. Slater, Stud. Surf. Sci. Catal. 168 (2007) 659–700. https://doi.org/10.1016/S0167-2991(07)80807-X

[28] R. Q. Snurr, A. T. Bell, D. N. Theodorou, J. Phys. Chem. B 97 (1993) 13742–13752. https://doi.org/10.1021/j100153a051

[29] K. Chihara, C. F. Mellot, A. K. Cheetham, S. Harms, H. Mangyo, M. Omote, R. Kamiyama, Korean J. Chem. Eng. 17 (2000) 649–651. https://doi.org/10.1007/BF02699112

[30] P. He, H. Liu, Y. Li, J. Zhu, S. Huang, Z. Lei, P. Wang, H. Tian, Adsorption, 18 (2012) 31–42. https://doi.org/10.1007/s10450-011-9378-7

[31] F. Zhao, X. Sun, R. Lu, L. Kang, Can. J. Chem. 95 (2017) 1241–1247. https://doi.org/10.1139/cjc-2017-0218

[32] B. Smit, T, L. M. Maesen, Chem. Rev. 108 (2008) 4125–4184. https://doi.org/10.1021/cr8002642

[33] A. P. Hawkins, A. Zachariou, S. F. Parker, P. Collier, N. Barrow, I. Silverwood, R. F. Howe, D. Lennon, RSC Adv., 10 (2020) 23136-23147. DOI: 10.1039/D0RA03871G

[34] S. Brunauer, P. H. Emmett, E. Teller. J. Am. Chem. Soc. 60 (1938) 309–319. https://doi.org/10.1021/ja01269a023

[35] W. Schmidt, U. Wilczok, C. Weidenthaler, O. Medenbach, R. Goddard, G.Buth, A. Cepak, J. Phys. Chem. B 111 (2007) 13538–13543. https://doi.org/10.1021/jp075934p

[36] Walter Loewenstein, American Mineralogist, 39 (1954) 92–96.

[37] N. G. Limas, T. A. Manz, RSC Adv. 6 (2016) 45727–45747. https://doi.org/10.1039/c6ra05507a

[38] A. Gonis, A. Meike, P. E. A. Turchi, K. Razan, Properties of Complex Inorganic Solids 2, California, January 1997.

[39] D. J. Chadi, Phys. Rev. B 16 (1977) 1746–1747. https://doi.org/10.1103/PhysRevB.16.1746

[40] M. Ernzerhof, G. E. Scuseria, J. Chem. Phys. 110 (1999) 5029–5036. https://doi.org/10.1063/1.478401

[41] P. Pulay, Chem. Phys. Lett. 73 (1980) 393–398. https://doi.org/10.1016/0009-2614(80)80396-4

[42] K. P. Schröder, J. Sauer, M. Leslie, C. Richard, A. Catlow, J. M. Thomas, Chem. Phys. Lett. 88 (1992) 320–325. https://doi.org/10.1016/0009-2614(92)90030-Q

[43] A. A. Shubin, C. R. A. Catlow, J. M. Thomas, K. I. Zamaraev, Proc. R. Soc. Lond. A. 446 (1994) 411–427. https://doi.org/10.1098/rspa.1994.0112

[44] C. Blanco, S. M. Auerbach. J. Phys. Chem. B 107 (2003) 2490-2499. https://doi.org/10.1021/jp026959l

[45] N. Raj, G. Sastre, C. R. A. Catlow, J. Phys. Chem. B 103 (1999) 11007–11015. https://doi.org/10.1021/jp991314f

[46] G. Sastre, C. R. A. Catlow, A. Corma, J. Phys. Chem. B 103(1999) 5187–5196. ttps://doi.org/10.1021/jp984776m

[47] K. P. Schröder, J. Sauer, J. Phys. Chem. 100 (1996) 11043–11049. https://doi.org/10.1021/jp953405s

[48] A. V. Brukhno, T. L. Underwood, Stratford, S. C. Parker, A. Purton, N. B. Wilding, Mol. Simul. 47 (2021) 131–151. https://doi.org/10.1080/08927022.2019.1569760

[49] A. Olivei, J. Phys. D. Appl. Phys. 9 (1976)183–195. https://doi.org/10.1088/0022-3727/9/2/008

[50] N. Metropolis, A. W. Rosenbluth, M. N. Rosenbluth, A. H. Teller, E. Teller, J. Chem. Phys. 21 (1953) 1087–1092. https://doi.org/10.1063/1.1699114

[51] B. J. Schulz, K. Binder, M. Müller, D. P. Landau, Phys. Rev. E 67 (2003) 067102. https://doi.org/10.1103/PhysRevE.67.067102

[52] Y. He, N. A. Seaton, Langmuir. 21 (2005) 8297–8301. https://doi.org/10.1021/la050694v

[53] P. Wang, Z. Qin, Y. Chen, M. Dong, J. Li, K. Zhang, P. Liu, J. Wang, W. Fan, ACS Catal. 8 (2018) 5485–5505. https://doi.org/10.1021/acscatal.8b01054.

[54] C. M. Wang, Y. D. Wang, Y. J. Du, G. Yang, Z. K. Xie, Catal. Sci. & Technol. 6 (2016) 3279-3288.
[55] J. P. Perdew, K. Burke, M. Ernzerhof, Phys. Rev. Lett. 77 (1996) 3865–3868.
[56] G. Kresse, J. Furthmüller, Phys. Rev. B 54 (1996) 11169–11186.
[57] G. Kresse, J. Hafner, Phys. Rev. B 47 (1993), 558–561.
[58] G. Kresse, J. Furthmüller, J. Comput. Mater. Sci. 6 (1996) 15–50.
[59] P. E. Blöchl, Phys. Rev. B 50 (1994) 17953–17979.
[60] S. Grimme, J. Antony, S. Ehrlich, H. Krieg, J. Chem. Phys. 132 (2010) 154104.
[61] S. Grimme, J. Comput. Chem. 27 (2006) 1787–1799.
[62] P. E. Blöchl, O. Jepsen, O. K. Andersen, Phys. Rev. B 49 (1994) 16223–16233.
[63] P. Sherwood, (2013) ChemShell, a Computational Chemistry Shell.
[64] Y. Lu, M. R. Farrow, P. Fayon, A. J. Logsdail, A. A. Sokol, C. R. A. Catlow, P. Sherwood, T. W. Keal, J. Chem. Theory Comput. 15 (2019), 1317–1328.
[65] S. A. F. Nastase, A. J. O'Malley, C. R. A. Catlow, A. J. Logsdail, Phys. Chem. Chem. Phys. 21 (2019) 2639–2650.
[66] A. J. O'Malley, A. J. Logsdail, A. A. Sokol, C. R. A. Catlow, Faraday Discuss. 188, (2016) 235–255.
[67] G. Artioli, C. Lamberti, G. L. Marra, Acta Crystallogr. Sect. B: Struct. Sci. 56 (2000) 2-10.
[68] W. Smith, C. W. Yong, P. M. Rodger, Mol. Simul. 28 (2002) 385–471.
[69] J. R. Hill, J. Sauer, J. Phys. Chem. 99 (1995) 1238-1244.
[70] F. Neese, Interdiscip. Rev. Comput. Mol. Sci. 2 (2012) 73-78.
[71] S. M. Campbell, D. M. Bibby, J. M. Coddington, R. F. Howe, R. H. Meinhold, J. Catal. 161 (1996) 338–349, https://doi.org/10.1006/jcat.1996.0191
[72] L. H. Ong, M. Dömök, R. Olindo, A. C. Van Veen, J. A. Lercher, Microporous Mesoporous Mater. 164 (2012) 9–20. https://doi.org/10.1016/j.micromeso.2012.07.033.
[73] K. S. W. Sing, D. H. Everett, R. A. W. Haul, L. Moscou, R. A. Pioretti, J. Rouquerol, Pure & App. Chem. 57 (1985), 603—619. https://doi.org/10.1351/pac198557040603
[74] M. S. Kumar, J. Pérez-Ramírez, M. N. Debbagh, B. Smarsly, U. Bentrup, A. Brückner, Appl. Catal. B Environ. 62 (2006) 244–254. https://doi.org/10.1016/j.apcatb.2005.07.012
[75] Y. Xiao, Y. Xiao, G. He, M. Yuan, Ind. Eng. Chem. Res. 57 (2018) 14254–14260. https://doi.org/10.1021/acs.iecr.8b04076
[76] S. Brunauer, The Adsorption of Gases and Vapors, Oxford University Press, p. 49, 1943.

[77] S. Wang, Y. He, W. Jiao, J. Wang, W. Fan, Current Opinion in Chem. Eng. 23 (2019) 146-154. https://doi.org/10.1016/j.coche.2019.04.002

[78] Michael Zeets, Daniel E. Resasco, Bin Wang. Catalysis Today. 312(2018) 44-50. https://doi.org/10.1016/j.cattod.2018.02.054.

[79] Ashley T. Smith, Philipp N. Plessow, and Felix Studt. J. Phys. Chem. C 125(2021), 37, 20373–20379. https://doi.org/10.1021/acs.jpcc.1c06670.

[80] Sen Wang, Pengfei Wang, Zhangfeng Qin, Yanyan chen, Mei Dong, Junfen Li, Kan Zhang, Ping Liu, Jianguo Wang, and Weibin Fan. ACS Catal. 8(2018), 6, 5485–5505. https://doi.org/10.1021/acscatal.8b01054

[81] S. Wang, S. Li, L. Zhang, Z. Qin, Y. Chen, M. Dong, J. Li, W. Fan and J. Wang. Catal. Sci. Technol., 8(2018), 3193-3204. https://doi.org/10.1039/C8CY00296G.

[82] C. G. Pope, J. Chem. Soc. Faraday Trans. 89 (1993) 1139–1141.
doi: 10.1039/FT9938901139.